Drastic field-induced resistivity upturns as signatures of unconventional magnetism in superconducting iron chalcogenides

Z. Zajicek,[1] I. Paulescu,[1] P. Reiss,[1,*] R. M. Abedin,[1] K. Sun,[1] S. J. Singh,[1,†] A. A. Haghighirad,[1,2] and A. I. Coldea[1,‡]

[1]Clarendon Laboratory, Department of Physics, University of Oxford, Parks Road, Oxford OX1 3PU, United Kingdom

[2]Institute for Quantum Materials and Technologies, Karlsruhe Institute of Technology, 76021 Karlsruhe, Germany

(Received 4 August 2025; revised 23 December 2025; accepted 2 January 2026; published 17 February 2026)

Electronic scattering is a powerful tool to identify underlying changes in electronic behavior and incipient electronic and magnetic orders. The nematic and magnetic phases are strongly intertwined under applied pressure in FeSe, however, the additional isoelectronic substitution of sulfur offers an elegant way to separate them. Here we report the detailed evolution of the electronic and superconducting behavior of $FeSe_{0.96}S_{0.04}$ under applied pressure via longitudinal magnetoresistance studies up to 15 T. At intermediate pressures, inside the nematic phase, the resistivity displays an upturn in zero magnetic field, which is significantly enhanced in the magnetic field, suggesting the stabilization of a spin-density wave phase, which competes with superconductivity. At higher pressures, beyond the nematic phase boundaries, the resistivity no longer displays any clear anomalies in the zero magnetic field, but an external magnetic field induces significant upturns in resistivity reflecting a field-induced order, where superconductivity and magnetic anomalies are enhanced in tandem. This study highlights the essential role of high magnetic fields in stabilizing different electronic phases and revealing a complex interplay between magnetism and superconductivity tuned by applied pressure in $FeSe_{1-x}S_x$.

DOI: 10.1103/gbfx-x9w1

I. INTRODUCTION

The phase diagrams of unconventional high-T_c superconductors are often complex with multiple competing electronic phases [1]. High magnetic fields at low temperatures are extremely important for understanding the interplay of these phases, as they can suppress the superconducting phases and reveal the underlying electronic states from which they emerge and access Fermi surfaces via quantum oscillations [2]. Resistivity upturns under applied magnetic fields at low temperatures are linked to signatures of potential competing orders with superconductivity [3]. One prominent mechanism that gives such upturns in electronic transport is the weak localization effect, where quantum interference enhances backscattering due to disorder [4] or the Kondo effect, where conduction electrons scatter off localized magnetic moments [5]. Additionally, the presence of charge or spin-density wave may lead to resistivity upturns due to partial gapping of the Fermi surfaces [6–8]. On the other hand, magnetic freezing effects from disordered magnetic moments can enhance resistivity, such as in spin glasses [9], whereas the formation of short-range magnetic order also lead to resistivity upturns, particularly in strongly correlated systems [10] or cuprate superconductors [11,12].

The pressure-induced high-T_c superconductivity of FeSe is a particular example where intertwined nematic electronic order and magnetism are particularly relevant for stabilizing superconductivity [13–15]. At ambient pressure, FeSe has a nematic electronic phase, induced by orbitally dependent electronic correlations, and a highly anisotropic superconducting phase is found below 9 K [16,17]. Despite the absence of any long-range magnetic order in FeSe, there is a competition between Néel and stripe spin fluctuations [18]. Applied pressure suppresses the nematic phase of FeSe and stabilizes a complex magnetic order [19]. Superconductivity is significantly enhanced, reaching a maximum T_c of 37 K at high pressures and spin fluctuations are proposed to mediate the superconducting pairing [14,15].

The electronic nematic phase of FeSe is highly sensitive to both chemical substitution in the Fe plane, such as the substitution of Cu, and also out of the plane at the chalcogen position with the isovalent substitution of sulfur or tellurium on selenium sites [20–23]. The nematic phase of $FeSe_{1-x}S_x$ is suppressed beyond $x = 0.18$, while superconductivity develops a small dome inside it and suffers significant changes in the gap symmetry inside the tetragonal phase [20,24]. The phase diagram of $FeSe_{1-x}S_x$ can be altered by combining applied and chemical pressure, by continuously suppressing the nematic phases and stabilizing enhanced superconductivity at high pressures [25,26]. In these systems, anomalies in resistivity, associated with a spin-density wave (SDW), occur over a broad regime under pressure in FeSe (∼8 to 63 kbar) [15], but with increasing x this magnetic region

*Present address: Max Planck Institute for Solid State Research, Stuttgart, Germany.

†Present address: Institute of High-Pressure Physics, Polish Academy of Sciences, Sokolowska 29/37, 01-142 Warsaw, Poland.

‡Contact author: amalia.coldea@physics.ox.ac.uk

narrows down (centered around 50 kbar for $x \sim 0.11$) [25]. This may indicate that the nature of the magnetic order in $FeSe_{1-x}S_x$ at low pressure, inside the nematic phase [27], may be distinct from that found at higher pressure in the tetragonal phase [25]. Thus, studying these systems in a detailed manner under pressure and high magnetic fields offers a unique insight into the role of isoelectronic substitution in affecting different competing interactions that influence superconductivity.

In this paper, we present a detailed transport study of $FeSe_{0.96}S_{0.04}$ under applied pressure to understand the stabilization of field-induced electronic phases and their interplay with superconductivity. Under applied pressure, the resistivity develops a sharp upturn in zero magnetic field, which reflects the stabilization of a spin-density wave inside the nematic phase. At higher pressures, the upturn disappears and, instead, the transition from the normal to the superconducting phase becomes broader. However, the presence of a magnetic field induces a large magnetoresistance, and the upturn in resistivity persists over the whole pressure range, indicating the development of field-induced electronic phases. The phase diagram suggests that superconductivity has two different domes that potentially reflect magnetically mediated pairing originating from different magnetic phases.

II. EXPERIMENTAL METHODS

Single crystals of $FeSe_{0.96}S_{0.04}$ were prepared using the chemical vapour transport method with $KCl/AlCl_3$ [29,30]. High-quality single crystals, considered for their sharp superconducting transitions and a high residual resistivity ratio, defined as $RRR = \rho_{xx}(300\text{ K})/\rho_{xx}$ (10 K). Transport experiments were carried out in constant magnetic field on different samples of the same batch: for sample S1 ($RRR \sim 18.7$) up to 16 T and for sample S2 ($RRR \sim 21.3$) in 15 T. For sample S2, measurements in constant field were performed using different field polarities and the data were symmetrized afterwards to eliminate any effect of mixing resistivity components. A maximum a.c. current of 1 mA was applied to the sample, and the magnetic field of up to 16 T for sample S1 and 15 T for sample S2 is aligned along the c direction and perpendicular to the applied current, thus probing the transverse magnetoresistance. Transport measurements in constant magnetic fields for sample S2 were performed using different field polarities, and the data were symmetrized afterwards to eliminate any effect of mixing resistivity components. Samples were pressurized using a commercially available BeCu pressure cell up to 20 kbar and cooling down slowly to 2 K at a rate of 0.5 K/min, inside a 16 T PPMS (Physical Property Measurement System). Daphne 7373 was used as the pressurising medium, which is hydrostatic up to 22 kbar [31]. The pressure was determined in situ using the superconducting transition temperature of tin at a slow cooling rate of 0.02 K/min.

III. TRANSPORT BEHAVIOR UNDER PRESSURE IN ZERO-MAGNETIC FIELD

Figures 1(a) and 1(b) show the evolution of resistivity with applied pressure for $FeSe_{0.96}S_{0.04}$ for sample S1 and sample S2, respectively. At ambient pressure, the resistivity displays a metallic-like behavior until the system enters the superconducting state below $T_c = 9.3$ K. A kink in resistivity at $T_s = 80(2)$ K for sample S1 defines the onset of the nematic electronic phase, which is also accompanied by a tetragonal-orthorhombic transition. By applying pressure up to $p_1 = 7.5$ kbar, the resistivity is continuously suppressed inside the nematic phase [see Fig. 1(c)], but resistivity variation as a function of temperature is much weaker due to the potential scattering from nematic domains. At higher pressures inside the nematic phase for $T_s < 40$ K, the resistivity develops an upturn at T_{MI} and a local maximum at T_p in the absence of the magnetic field [see also Fig. 2(a)]. Resistivity upturns in zero-magnetic field were previously detected in interplane resistance, ρ_{zz} for $x = 0.043$ [27] and a thin 2.3 μm flake [32]. Such a feature was associated with a magnetic phase transition driven by a spin-density wave (SDW) in FeSe [15]. Once the nematic phase is suppressed above $p_2 \sim 13.8$ kbar, the resistivity upturn is washed out while

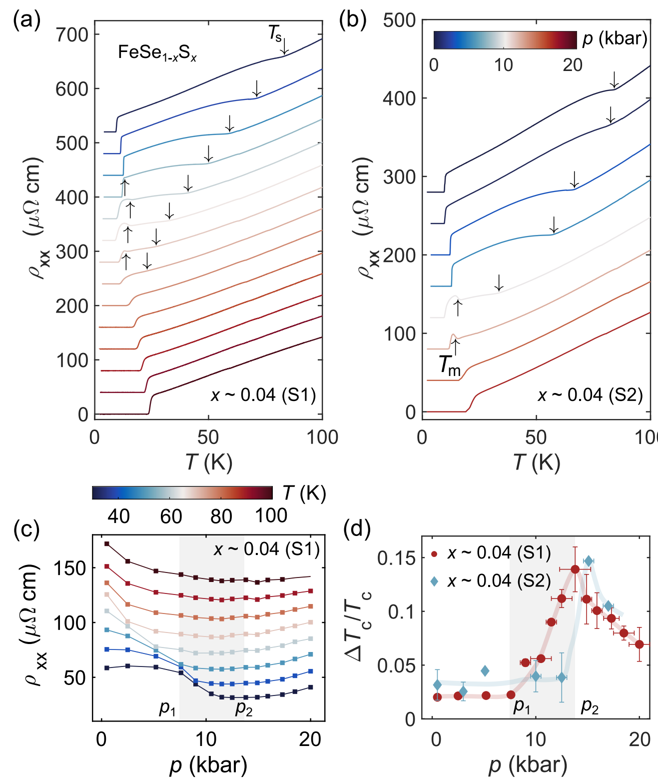

FIG. 1. The evolution of the transport behavior under pressure in $FeSe_{0.96}S_{0.04}$. (a) and (b) Longitudinal resistivity ρ_{xx} against temperature tuned under different applied pressure for samples S1 and S2. The down arrows mark the nematic transition temperature at T_s, whereas the up arrows indicate the minimum in the first-order derivative at T_m. The curves are shifted vertically for easier visualization. (c) The pressure dependence of the resistivity at different fixed temperatures. Shaded gray areas indicate boundaries between different electronic phases at p_1 and p_2. (d) The relative changes in the superconducting transition width, $\Delta T_c/T_c = (T_{c,\text{mid}} - T_{c,\text{off}})/T_{c,\text{mid}}$, where $T_{c,\text{mid}}$ is defined as the peak in first derivative (see Fig. S1 in the SM [28]) versus applied pressure for samples S1 (solid circles) and S2 (solid diamonds). Shaded gray areas indicate phase boundaries between different electronic phases at p_1 and p_2.

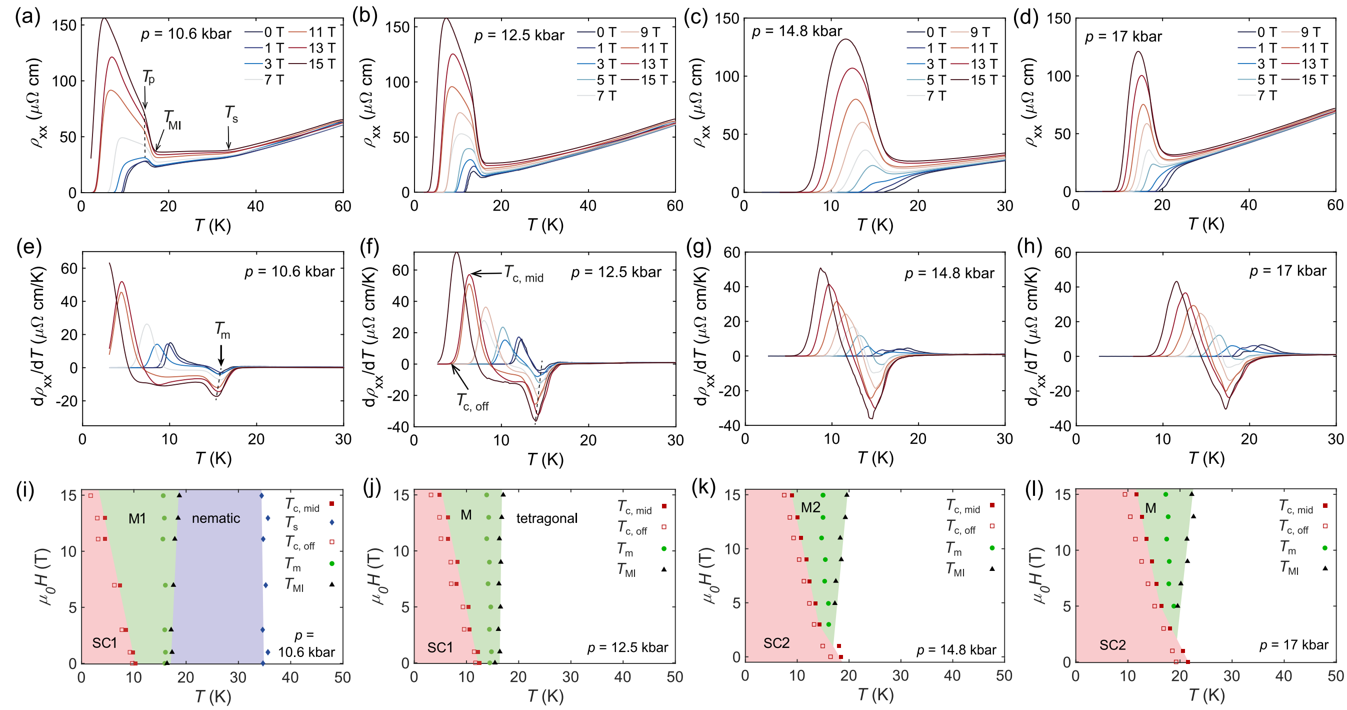

FIG. 2. The magnetoresistance of $FeSe_{0.96}S_{0.04}$ for sample S2 tuned by applied pressure. (a)–(d) Temperature dependence of the longitudinal resistivity in magnetic fields of up to 15 T under pressures equal to or greater than $p_1 \sim 10.6$ kbar. (e)–(h) The corresponding first derivatives of ρ_{xx} with respect to temperature related to raw data in panels (a)–(d). The development of the new field-induced phase is defined as the minimum in the derivative at T_m and the local minimum in resistivity data at T_{MI}, whereas critical temperature is defined here as the maximum in the derivative at the midpoint transition, $T_{c,mid}$ (see Figs. S1 and S2 in the SM [28]). The magnetic field-temperature phase diagram indicating the different electronic phases, nematic (purple), magnetic M1 and M2 (green), superconducting SC1 and SC2 (red).

the superconducting transition width becomes broader [see Figs. 1(a), 1(b), and 1(d)].

To understand the trends in scattering under pressure, one can assess the changes in resistivity at constant temperature, as shown in Fig. 1(c). At high temperatures, the resistivity decreases smoothly with applied pressure, as expected, due to an increase in the electronic bandwidth. At temperatures below 100 K, the resistivity decreases with pressure inside the nematic phase, below p_1, but then increases in the tetragonal phase above p_2, suggesting significant changes in scattering, electronic correlations, or enhanced spin fluctuations [see Fig. 1(c)]. Interestingly, the temperature dependence of the resistivity in the high-pressure regime is rather linear and broadly similar to other $FeSe_{1-x}S_x$ [27,33], $Fe_{1-z}Cu_zSe$ [34], and FeSe [15], suggesting that the high-pressure phase is a different electronic phase with higher resistivity.

The width of the superconducting transition changes significantly with pressure, as shown in Fig. 1(d). In the low pressure regime, $p < p_1$, the superconducting transitions are sharp ($\Delta T_c \sim 0.5$ K). However, in the intermediate pressure regime, where signatures of magnetic order are found, the superconducting transition broadens significantly (close to 3 K, similar to previous studies in Cu-FeSe [34]). Relative changes in the superconducting transition, $\Delta T_c/T_c$, have a significant enhancement just outside the boundaries of the nematic phase close to p_2, which could suggest the presence of strong critical nematic or spin fluctuations [19,35], the existence of quantum Griffiths phases [35], or the manifestation of different competing electronic phases at high pressure.

IV. MAGNETOTRANSPORT BEHAVIOR UNDER APPLIED PRESSURE

High magnetic fields are used to suppress the superconducting phase and reveal anomalous transport behavior at low temperatures. Figure 2 describes the evolution with pressure of the temperature dependence of resistivity in different magnetic fields. At intermediate pressures ($p_1 < p < p_2$), the resistivity develops a metallic-to-insulating transition at T_{MI} and an additional slope change at T_p in magnetic field, coinciding with the zero-field resistance peak, as shown in Figs. 2(a) and 2(b). The change in magnetotoresistance in 15 T is rather weak inside the nematic phase below T_s (a factor of 1.5 at 20 K) before increasing significantly below T_{MI}, by a factor of 2.75 at 14 K. This suggests that the magnetic field has a significant influence on the low-temperature electronic phase.

The field-induced upturns in resistivity at low temperatures, once superconductivity is suppressed, closely resemble those previously observed in FeSe [36] and suggest stabilization of an SDW phase. Field-induced SDWs are often found in systems close to nesting instabilities, such as low-dimensional organics [37,38]. Below T_{MI}, resistivity has an activated-like behavior as a result of the opening of the SDW energy gap. A strong magnetoelastic coupling could be responsible for the change in slope at T_p, similar to FeSe, which displays an

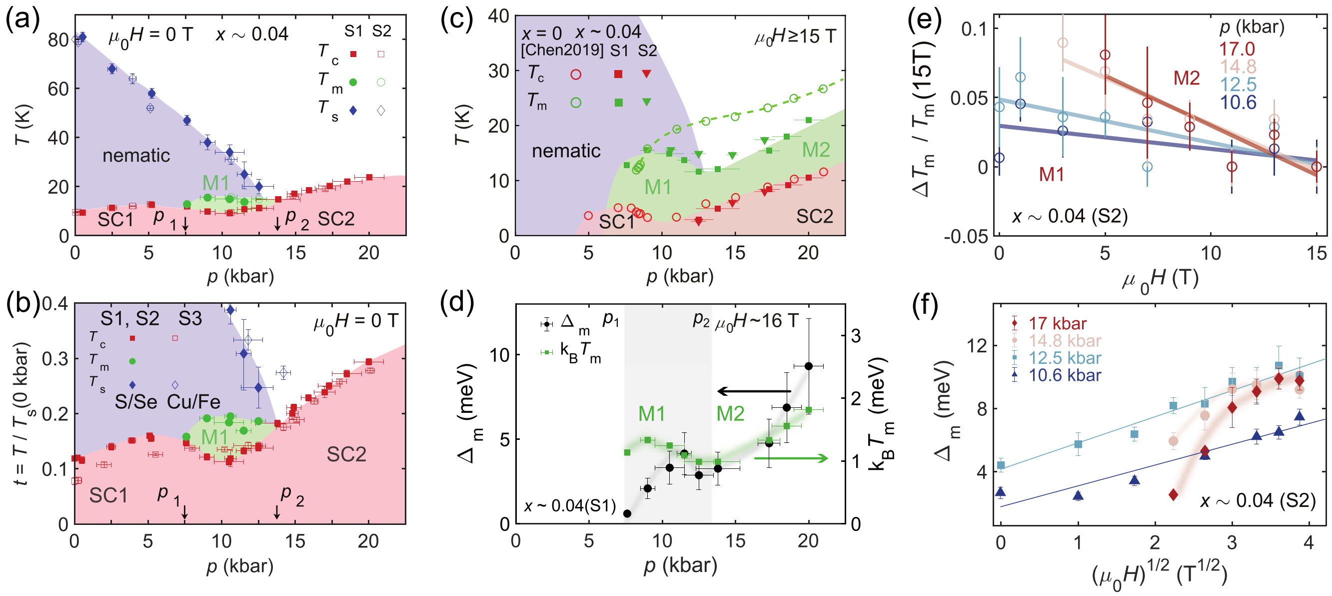

FIG. 3. Comparison of the $p - T$ phase diagrams and field-induced effects of $FeSe_{0.96}S_{0.04}$ under applied pressure. (a) Pressure-temperature phase diagram of $FeSe_{0.96}S_{0.04}$ for sample S1 (solid symbols) and sample S2 (open symbols) indicating the different competing electronic phases: nematic up to p_1 (purple area), magnetic (M1 green area) ($p_1 < p < p_2$) and superconducting (SC1 and SC2). (b) The phase diagram of $FeSe_{0.96}S_{0.04}$ and $Fe_{0.9975}Cu_{0.0025}Se$ (after Ref. [34]) in reduced temperature units in relation to their T_s, $t = T/T_s$. (c) Pressure-temperature phase diagram of FeSe and $FeSe_{0.96}S_{0.04}$ in magnetic fields. Symbols correspond to $FeSe_{0.96}S_{0.04}$ for samples S1 (solid green squares in 16 T) and S2 (solid triangles in 15 T) and FeSe (open circles in 16 T) after Ref. [41]. The green shaded region represents the magnetic phases in field (M1 and M2). (d) The pressure dependence of the effective activation energy, Δ_M (on the left y axis) together with k_BT_m in 16 T (on the right y axis). Δ_m is defined from the slope from $\log \rho$ versus $1/T$ (see Fig. S3 for S1 and Fig. S4 for S2 in the SM [28]). (e) The field dependence of the relative changes in the magnetic transition, $\Delta T_m/T_m = [T_m(\mu_0H) - T_m(15\text{ T})]/T_m(15\text{ T})$, where T_m is taken as the minimum in the first derivative [see Figs. 2(e)–2(h)]. (f) The variation of the effective activation energy, Δ_m, as a function of square root of magnetic field, $H^{0.5}$, for different pressures for sample S2 (see Figs. 2(a)–2(d) and Fig. S5 in the SM [28]). Solid lines are linear fits to the data and curved lines are guides to the eye.

additional increase of the in-plane lattice parameters around 15 kbar inside the nematic phase [39]. Interestingly, at higher pressures, $p > p_2$, despite the lack of any upturns in zero-magnetic field with much broader superconducting transitions [see Fig. 1(d)], we detect significant resistivity upturns induced by magnetic fields, similar to those observed at lower pressures. This reflects that a similar underlying mechanism is responsible for the large resistivity upturns and the corresponding significant magnetoresistance in these systems [see Figs. 2(c) and 2(d) and the corresponding derivatives in Figs. 2(g) and 2(h)].

The evolution of magnetic field-induced transitions at each pressure is quantified using the sharp minimum at T_m in the first derivative of resistivity as a function of temperature [see Figs. 2(e)–2(h)]. This characteristic temperature, T_m, decreases with increasing magnetic field as superconductivity is suppressed [see Figs. 2(i)–2(l)]. At intermediate pressure, the relative change in transition temperature, $\Delta T_m/T_m(15\text{ T})$ slightly decreases as the magnetic field increases [see Figs. 2(e)–2(h) and Fig. 3(e)]. On the other hand, at high pressures ($p > p_2$), the position of T_m is much more sensitive to magnetic fields, as shown in Fig. 3(e).

In high magnetic fields, in the temperature range just below T_{MI}, the resistivity increases exponentially as $\rho \sim \exp(\Delta_m/k_BT)$, and the effective activation energy, Δ_m, can be estimated from the slope of the natural logarithm of resistivity against the inverse temperature (see Figs. S3, S4 and S5 in the SM [28]). As a function of applied pressure, Δ_m closely follows the dependence of T_m, as shown in Fig. 3(d). To understand how a magnetic field induces changes in resistivity, we follow the evolution of Δ_m for sample S2 shown in Fig. 2. We find that Δ_m increases with the applied pressure and has a field dependence of the form $H^{0.5}$ with a similar slope inside the nematic phase ($p_1 < p < p_2$), as shown in Fig. 3(f). On the other hand, at high pressures, $p > p_2$, Δ_m is induced by magnetic fields and varies faster towards saturation, indicating a strong sensitivity to field (see Fig. S5 in the SM [28]). As Δ_m increases in magnetic field, the T_{MI} transition temperature shifts to higher values, as represented in the temperature-magnetic field phase diagrams at different pressures in Figs. 2(i)–2(l). The dependence of Δ_m shows similarities with the field-induced magnetism detected in underdoped $La_{2-x}Sr_xCuO_4$ ($x = 0.10$), where superconductivity and antiferromagnetism coexist [40].

When the magnetic order is accompanied by a tetragonal-orthorhombic transition, a first-order phase transition with hysteretic behavior is expected, as found in FeSe at high pressure [19,39,42,43]. We detect just a weak hysteresis at 12.5 kbar between the cooling and warming curves (using a rate of 0.5 K/min for sample S2), due to the magnetoelastic coupling at T_p inside the nematic phase. Therefore, the isoelectronic substitution of sulfur for selenium in FeSe likely suppresses the strength of interactions and reduces the coupling between the magnetic and orthorhombic distortion (see Fig. S6 in the SM [28]).

V. DISCUSSION

Figure 3(a) shows the pressure-temperature phase diagram for different single crystals of $FeSe_{0.96}S_{0.04}$ based on the zero-field resistivity data. This phase is split into three different regimes: the low-pressure nematic regime below $p < p_1$, the intermediate pressure regime, $p_1 < p < p_2$, where the resistivity has an upturn at T_m in the absence of the magnetic field inside the nematic phase, and the high-pressure regime for $p > p_2$, outside the nematic phase, where the resistivity increases and becomes progressively linear as a function of temperature [see Figs. 1(a) and 1(b)]. The superconductivity displays a two-dome structure as a function of pressure, and at intermediate pressures T_c decreases whereas T_m increases, suggesting a competition between the two phases. Even for systems with higher sulfur substitution, like in $FeSe_{0.89}S_{0.11}$ under pressure, two similar superconductivity domes emerge, without having any clear resistivity upturns in a zero magnetic field [33].

Figure 3(b) compares the zero-field phase diagram under pressure of $FeSe_{0.96}S_{0.04}$ for two different samples, S1 and S2, with that of $Fe_{1-z}Cu_zSe$ ($z = 0.0025$) previously reported in Ref. [34], both scaled by the nematic transition T_s at ambient pressure. At ambient pressure, sulfur substitution slightly enhances T_c, compared to FeSe, while Cu substitution suppresses T_c [23,34]. Importantly, the pressure variation of the nematic and superconducting transitions is rather similar for the two systems. However, in the intermediate pressure regime, the dome of magnetic order of $FeSe_{0.96}S_{0.04}$ is absent in $Fe_{1-z}Cu_zSe$, indicating that the increased impurity scattering potentially obscures the resistivity upturns in the absence of a magnetic field. Interestingly, in the high-pressure phase above $p_2 = 12.5$ kbar, the pressure variation of the superconducting transition temperature is comparable.

Figure 3(c) shows the low-temperature phase diagram of $FeSe_{0.96}S_{0.04}$ in an applied magnetic field of 15 T, compared to that of FeSe in 16 T from [41]. Magnetic fields suppress superconductivity and enhance the features associated with the emergence of magnetism, similar to FeSe under pressure [15,41,44]. However, the isoelectronic substitution with sulfur affects magnetic interactions and influences the location of different magnetic phases. Interestingly, in high magnetic fields of 15 T, the maximum in T_c for SC1 phase around 7.5 kbar coincides with the onset of the magnetic phase [see Fig. 3(a)]. However, at high magnetic fields and pressures, above p_2, the superconducting temperatures of FeSe and $FeSe_{0.96}S_{0.04}$ are rather similar, despite the reduction in T_m of $\sim$10 K. This suggests that the high-pressure superconductivity of iron-chalcogenide is robust, whereas the magnetic phase is more fragile, similar to that found in Cu-doped FeSe [34]. Both T_c and T_m increase with pressure, suggesting a potential coexistence between the high-pressure superconducting, SC2, and magnetic phase, M2.

The observed differences in resistivity upturns in high magnetic fields across the pressure phase diagram imply a clear distinction between a rather robust SDW order coupled with orthorhombic distortion inside the nematic phase, called the M1 phase with C_2 symmetry ($p_1 < p < p_2$), and a more fragile order outside the nematic phase defined as the M2 phase ($p > p_2$) [see Figs. 2(i)–2(l)]. Figure 3(d) shows that the pressure dependence of Δ_M (for sample S1) in 15 T closely follows the magnetic temperature, T_m of the M1 and M2 magnetic domes but its energy scale is much larger than $k_B T_m$, suggesting that the magnetic field significantly alters the SDW gap and scattering. Above p_2, the resistivity in zero-magnetic field becomes rather linear in temperature [see Figs. 1(a) and 1(b)] and the absolute value increases under pressure [see Fig. 1(c)], suggesting a change in electronic behaviour in the high-pressure regime associated with the field-induced M2 phase, similar to $FeSe_{0.89}S_{0.11}$ [26,33]. This differentiation in magnetism as a function of applied pressure can be caused by variations in size and lengthscale of spin fluctuations, as observed in $FeSe_{0.9}S_{0.1}$ using NMR studies [45]. The magnitude of $(1/T_1T)$ AFM spin fluctuations in $FeSe_{1-x}S_x$ was found to be larger inside the nematic phase (C_2 phase) as compared to the high-pressure phase outside the nematic phase (C_4 phase), despite the fact that AFM spin fluctuations are more effective in enhancing superconductivity in the absence of nematicity. Additionally, the AFM correlation length ξ_{AFM} was estimated to be longer inside the nematic phase [46].

The presence of two separate superconductivity domes suggests that the pairing mechanism changes under pressure in $FeSe_{0.96}S_{0.04}$ [see Figs. 3(a)–3(c)]. Inside the nematic phase, the superconductivity displays a minimum where the magnetic phase M1 has a maximum, suggesting a likely competition between the two of them. The robustness of the high-pressure superconducting phase, SC2, to different substitutions [2,34] indicates either s_{++} sign-preserving pairing or a complex superconducting phase coexisting with fragile magnetism inside the phase M2 [see Fig. 3(e)]. Surprisingly, the superconducting critical temperature at the nematic end point is not a maximum close to p_2, suggesting that nematic critical fluctuations may be quenched [33], there is an electronic phase coexistence or potential quantum Griffiths phases [35]. Close to p_2, the relative widths of the superconducting transitions, $\Delta T_c/T_c$, are enhanced [see Fig. 1(d)] and a weak hysteretic behavior can be detected in the magnetic field (see Fig. S6 in the SM [28]).

The nature of the magnetic order of FeSe is rather complex and varies with applied pressure. On one hand, at ambient pressure, the lack of long-range static order is explained due to the competition between Néel and stripe spin orders [18]. In the presence of applied strain, FeSe is detwined and promotes Néel C_4 symmetric low-energy magnetic excitations [47]. Applied pressure is predicted to change itinerant magnetism by shifting an additional d_{xy} hole pocket at the Fermi level [48]. Such a band shift would occur only if the height of the chalcogen increases above the conducting Fe planes, as in the case of the Te isoelectronic substitution [49]. On the other hand, μSR studies in FeSe under pressure postulate that the static magnetic order corresponds to the collinear (single-stripe) antiferromagnetic or bicollinear order [50]. Only local probes using Mössbauer and μSR spectroscopy detect a small ordered magnetic moment in FeSe of 0.2 μ_B at $p = 40$ kbar [39,51]). Moreover, the high-pressure superconductivity of FeSe may coexist with magnetic order [52].

Drastic changes in electronic behavior and scattering due to the development of novel electronic orders can be assessed from the resistivity behavior. Often in magnetic systems such as $BaFe_2As_2$, the resistivity decreases drastically at the onset of the SDW phase, as scattering by low-energy magnetic fluctuations is suppressed due to the opening of a magnetic energy gap [53,54]. Furthermore, the SDW order leads to the Fermi surface reconstruction induced by nesting between electron and hole pockets [55]. Indeed, a slow quantum oscillation was associated with a Fermi surface reconstruction in the SDW phase of FeSe under pressure [8]. The reduction of carrier density, n, due to reconstruction consequently has a much larger effect on resistivity which leads to resistivity upturns at low temperature, as observed in $FeSe_{1-x}S_x$ (see Figs. 1 and 2) and for Co, K, and P-substituted $BaFe_2As_2$ [53,54].

Changes in magnetoresistance and resistivity upturns reveal the nature of field-induced electronic phases as a function of applied pressure, both inside the M1 and M2 phases of $FeSe_{0.96}S_{0.04}$. At high pressure, the magnetoresistance is slowly reduced with increasing pressure and the magnetic transition temperature, whereas T_m, and Δ_m activation gap are highly sensitive to magnetic fields [see Fig. 3(e)]. Furthermore, magnetoresistance can be strongly suppressed in highly inhomogeneous phases, or by strong impurity scattering, as in the case of Cu substitution within the conducting Fe plane [23,34]. Thus, the high-pressure phase, due to the reduction in magnetoresistance and sensitivity of electronic transitions to high-magnetic field [see Figs. 3(e) and 3(f)], likely has magnetic regions with reduced correlation length, consistent with NMR studies [46].

VI. CONCLUSIONS

This study gives insight into the complex evolution of magnetic, nematic, and superconducting phases in $FeSe_{0.96}S_{0.04}$ tuned by pressure. External magnetic fields reveal large resistivity upturns as signatures of Fermi surface reconstruction and activated behavior. The phase diagrams under pressure reveal two different superconducting and magnetic regimes reflecting the competition or coexistence between these electronic phases. Firstly, inside the nematic phase, at intermediate pressure, the resistivity upturns are consistent with the development of the SDW phase, and the superconductivity is weakened where the SDW is enhanced, suggesting a competition between them. Secondly, at high pressures, resistivity upturns are induced by the magnetic field, due to fragile magnetism, which coexist with superconductivity. The high-pressure superconductivity remains robust to different chemical substitutions, supporting a sign-preserving s_{++} pairing symmetry. Our study emphasizes the important role of magnetic fields in inducing and probing electronic orders under applied pressure in unconventional superconductors.

ACKNOWLEDGMENTS

This work was mainly supported by Engineering and Physical Sciences Research Council (EPSRC) (EP/I004475/1) and Oxford Centre for Applied Superconductivity. We also acknowledge financial support of the John Fell Fund of the Oxford University. Z.Z. acknowledges financial support from the EPSRC studentship (EP/N509711/1 and EP/R513295/1). R.M.A. acknowledges funding from the Margaret Thatcher Scholarship Trust. I.P. acknowledges funding for an iCASE Studentship (EP/W524311/1) and additional sponsorship from Oxford Instruments. P.R. and A.A.H. acknowledge financial support of the Oxford Quantum Materials Platform Grant (EP/M020517/1). A.A.H. acknowledges support of the Deutsche Forschungsgemeinschaft (DFG; German Research Foundation) under CRC/TRR 288 for Project-ID 422213477-TRR 288 (Project No. B03). A.I.C. acknowledges an EPSRC Career Acceleration Fellowship (EP/I004475/1) and the EPSRC Centre for Doctoral Training in Superconductivity (EP/Y035453/1).

DATA AVAILABILITY

The data that support the findings of this study will be made available through the open access data archive at the University of Oxford (ORA) [56].

[1] R. M. Fernandes, A. I. Coldea, H. Ding, I. R. Fisher, P. Hirschfeld, and G. Kotliar, Iron pnictides and chalcogenides: A new paradigm for superconductivity, Nature (London) **601**, 35 (2022).

[2] Z. Zajicek, P. Reiss, D. Graf, J. C. A. Prentice, Y. Sadki, A. A. Haghighirad, and A. I. Coldea, Unveiling the quasiparticle behavior in the pressure-induced high-T_c phase of an iron-chalcogenide superconductor, npj Quantum Mater. **9**, 52 (2024).

[3] W. Chen, B. M. Andersen, and P. J. Hirschfeld, Theory of resistivity upturns in metallic cuprates, Phys. Rev. B **80**, 134518 (2009).

[4] G. Bergmann, Weak localization in thin films: A time-of-flight experiment with conduction electrons, Phys. Rep. **107**, 1 (1984).

[5] J. Kondo, Resistance minimum in dilute magnetic alloys, Prog. Theor. Phys. **32**, 37 (1964).

[6] G. Grüner, The dynamics of charge-density waves, Rev. Mod. Phys. **60**, 1129 (1988).

[7] E. Zhang, D. Peng, Y. Zhu, L. Chen, B. Cui, X. Wang, W. Wang, Q. Zeng, and J. Zhao, Bulk superconductivity in pressurized trilayer nickelate $Pr_4Ni_3O_{10}$ single crystals, Phys. Rev. X **15**, 021008 (2025).

[8] T. Terashima, N. Kikugawa, A. Kiswandhi, E.-S. Choi, J. S. Brooks, S. Kasahara, T. Watashige, H. Ikeda, T. Shibauchi, Y. Matsuda, T. Wolf, A. E. Böhmer, F. Hardy, C. Meingast, H. v. Löhneysen, M.-T. Suzuki, R. Arita, and S. Uji, Anomalous Fermi surface in FeSe seen by Shubnikov-de Haas oscillation measurements, Phys. Rev. B **90**, 144517 (2014).

[9] J. A. Mydosh, *Spin Glasses: An Experimental Introduction* (CRC Press, London, 1993).

[10] E. Dagotto, T. Hotta, and A. Moreo, Nanoscale phase separation and colossal magnetoresistance: The physics of manganites and related compounds, Phys. Rep. **344**, 1 (2001).

[11] P. Bourgeois-Hope, S. Y. Li, F. Laliberté, S. Badoux, S. M. Hayden, N. Momono, T. Kurosawa, K. Yamada, H. Takagi, N. Doiron-Leyraud, and L. Taillefer, Link between magnetism and resistivity upturn in cuprates: A thermal conductivity study of $La_{2-x}Sr_xCuO_4$, arXiv:1910.08126.

[12] G. S. Boebinger, Y. Ando, A. Passner, T. Kimura, M. Okuya, J. Shimoyama, K. Kishio, K. Tamasaku, N. Ichikawa, and S. Uchida, Insulator-to-metal crossover in the normal state of $La_{2-x}Sr_xCuO_4$ near optimum doping, Phys. Rev. Lett. **77**, 5417 (1996).

[13] Y. Mizuguchi, F. Tomioka, S. Tsuda, T. Yamaguchi, and Y. Takano, Superconductivity at 27 K in tetragonal FeSe under high pressure, Appl. Phys. Lett. **93**, 152505 (2008).

[14] S. Medvedev, T. M. McQueen, I. A. Troyan, T. Palasyuk, M. I. Eremets, R. J. Cava, S. Naghavi, F. Casper, V. Ksenofontov, G. Wortmann, and C. Felser, Electronic and magnetic phase diagram of β-$Fe_{1.01}Se$ with superconductivity at 36.7 K under pressure, Nat. Mater. **8**, 630 (2009).

[15] J. P. Sun, K. Matsuura, G. Z. Ye, Y. Mizukami, M. Shimozawa, K. Matsubayashi, M. Yamashita, T. Watashige, S. Kasahara, Y. Matsuda, J.-Q. Yan, B. C. Sales, Y. Uwatoko, J.-G. Cheng, and T. Shibauchi, Dome-shaped magnetic order competing with high-temperature superconductivity at high pressures in FeSe, Nat. Commun. **7**, 12146 (2016).

[16] F.-C. Hsu, J.-Y. Luo, K.-W. Yeh, T.-K. Chen, T.-W. Huang, P. M. Wu, Y.-C. Lee, Y.-L. Huang, Y.-Y. Chu, D.-C. Yan, and M.-K. Wu, Superconductivity in the PbO-type structure α-FeSe, Proc. Natl. Acad. Sci. USA **105**, 14262 (2008).

[17] P. O. Sprau, A. Kostin, A. Kreisel, A. E. Böhmer, V. Taufour, P. C. Canfield, S. Mukherjee, P. J. Hirschfeld, B. M. Andersen, and J. C. S. Davis, Discovery of orbital-selective Cooper pairing in FeSe, Science **357**, 75 (2017).

[18] Q. Wang, Y. Shen, B. Pan, X. Zhang, K. Ikeuchi, K. Iida, A. D. Christianson, H. C. Walker, D. T. Adroja, M. Abdel-Hafiez, X. Chen, D. A. Chareev, A. N. Vasiliev, and J. Zhao, Magnetic ground state of FeSe, Nat. Commun. **7**, 12182 (2016).

[19] E. Gati, A. E. Böhmer, S. L. Bud'ko, and P. C. Canfield, Bulk superconductivity and role of fluctuations in the iron-based superconductor FeSe at high pressures, Phys. Rev. Lett. **123**, 167002 (2019).

[20] A. I. Coldea, S. F. Blake, S. Kasahara, A. A. Haghighirad, M. D. Watson, W. Knafo, E. S. Choi, A. McCollam, P. Reiss, T. Yamashita, M. Bruma, S. Speller, Y. Matsuda, T. Wolf, T. Shibauchi, and A. J. Schofield, Evolution of the low-temperature Fermi surface of superconducting $FeSe_{1-x}S_x$ across a nematic phase transition, npj Quantum Mater. **4**, 2 (2019).

[21] Y. Mizuguchi, F. Tomioka, S. Tsuda, T. Yamaguchi, and Y. Takano, Substitution effects on FeSe superconductor, J. Phys. Soc. Jpn. **78**, 074712 (2009).

[22] K. Mukasa, K. Matsuura, M. Qiu, M. Saito, Y. Sugimura, K. Ishida, M. Otani, Y. Onishi, Y. Mizukami, K. Hashimoto, J. Gouchi, R. Kumai, Y. Uwatoko, and T. Shibauchi, High-pressure phase diagrams of $FeSe_{1-x}Te_x$: Correlation between suppressed nematicity and enhanced superconductivity, Nat. Commun. **12**, 381 (2021).

[23] Z. Zajicek, S. J. Singh, H. Jones, P. Reiss, M. Bristow, A. Martin, A. Gower, A. McCollam, and A. I. Coldea, Drastic effect of impurity scattering on the electronic and superconducting properties of Cu-doped FeSe, Phys. Rev. B **105**, 115130 (2022).

[24] T. Hanaguri, V. Iwaya, Y. Kohsaka, T. Machida, T. Watashige, S. Kasahara, T. Shibauchi, and Y. Matsuda, Two distinct superconducting pairing states divided by the nematic end point in $FeSe_{1-x}S_x$, Sci. Adv. **4**, eaar6419 (2018).

[25] K. Matsuura, Y. Mizukami, Y. Arai, Y. Sugimura, N. Maejima, A. Machida, T. Watanuki, T. Fukuda, T. Yajima, Z. Hiroi, K. Y. Yip, Y. C. Chan, Q. Niu, S. Hosoi, K. Ishida, K. Mukasa, S. Kasahara, J.-G. Cheng, S. K. Goh, Y. Matsuda, *et al.*, Maximizing T_c by tuning nematicity and magnetism in $FeSe_{1-x}S_x$ superconductors, Nat. Commun. **8**, 1143 (2017).

[26] P. Reiss, A. McCollam, Z. Zajicek, A. A. Haghighirad, and A. I. Coldea, Collapse of metallicity and high-T_c superconductivity in the high-pressure phase of $FeSe_{0.89}S_{0.11}$, npj Quantum Mater. **9**, 73 (2024).

[27] L. Xiang, U. S. Kaluarachchi, A. E. Böhmer, V. Taufour, M. A. Tanatar, R. Prozorov, S. L. Bud'ko, and P. C. Canfield, Dome of magnetic order inside the nematic phase of sulfur-substituted FeSe under pressure, Phys. Rev. B **96**, 024511 (2017).

[28] See Supplemental Material at http://link.aps.org/supplemental/10.1103/gbfx-x9w1 for further details about the extraction of different parameters from resistivity data.

[29] D. Chareev, E. Osadchii, T. Kuzmicheva, J.-Y. Lin, S. Kuzmichev, O. Volkova, and A. Vasiliev, Single crystal growth and characterization of tetragonal $FeSe_{1-x}$ superconductors, CrystEngComm **15**, 1989 (2013).

[30] A. E. Böhmer, V. Taufour, W. E. Straszheim, T. Wolf, and P. C. Canfield, Variation of transition temperatures and residual resistivity ratio in vapor-grown FeSe, Phys. Rev. B **94**, 024526 (2016).

[31] K. Yokogawa, K. Murata, H. Yoshino, and S. Aoyama, Solidification of high-pressure medium Daphne 7373, Jpn. J. Appl. Phys. **46**, 3636 (2007).

[32] J. Xie, X. Liu, W. Zhang, S. M. Wong, X. Zhou, Y. Zhao, S. Wang, K. T. Lai, and S. K. Goh, Fragile pressure-induced magnetism in FeSe superconductors with a thickness reduction, Nano Lett. **21**, 9310 (2021).

[33] P. Reiss, D. Graf, A. A. Haghighirad, W. Knafo, L. Drigo, M. Bristow, A. Schofield, and A. I. Coldea, Quenched nematic criticality and two superconducting domes in an iron-based superconductor, Nat. Phys. **16**, 89 (2020).

[34] Z. Zajicek, S. J. Singh, and A. I. Coldea, Robust superconductivity and fragile magnetism induced by the strong Cu impurity scattering in the high-pressure phase of FeSe, Phys. Rev. Res. **4**, 043123 (2022).

[35] P. Reiss, D. Graf, A. A. Haghighirad, T. Vojta, and A. I. Coldea, Signatures of a quantum Griffiths phase close to an electronic nematic quantum phase transition, Phys. Rev. Lett. **127**, 246402 (2021).

[36] T. Terashima, N. Kikugawa, S. Kasahara, T. Watashige, Y. Matsuda, T. Shibauchi, and S. Uji, Magnetotransport study of the pressure-induced antiferromagnetic phase in FeSe, Phys. Rev. B **93**, 180503 (2016).

[37] A. V. Kornilov, V. M. Pudalov, Y. Kitaoka, K. Ishida, T. Mito, J. S. Brooks, J. S. Qualls, J. A. A. J. Perenboom, N. Tateiwa, and T. C. Kobayashi, Novel phases in the field-induced spin-density-wave state in $(TMTSF)_2PF_6$, Phys. Rev. B **65**, 060404 (2002).

[38] B. Korin-Hamzić, M. Basletić, A. Hamzić, and K. Bechgaard, Change of the activation energy in the SDW state of $(TMTSF)_2PF_6$, Synth. Met. **103**, 2125 (1999).

[39] K. Kothapalli, A. E. Böhmer, W. T. Jayasekara, B. G. Ueland, P. Das, A. Sapkota, V. Taufour, Y. Xiao, E. Alp, S. L. Bud'ko, P. C. Canfield, A. Kreyssig, and A. I. Goldman, Strong cooperative coupling of pressure-induced magnetic order and nematicity in FeSe, Nat. Commun. **7**, 12728 (2016).

[40] B. Lake, H. M. Rønnow, N. B. Christensen, G. Aeppli, K. Lefmann, D. F. McMorrow, P. Vorderwisch, P. Smeibidl, N. Mangkorntong, T. Sasagawa, M. Nohara, H. Takagi, and T. E. Mason, Antiferromagnetic order induced by an applied magnetic field in a high-temperature superconductor, Nature (London) **415**, 299 (2002).

[41] G.-Y. Chen, E. Wang, X. Zhu, and H.-H. Wen, Synergy and competition between superconductivity and antiferromagnetism in FeSe under pressure, Phys. Rev. B **99**, 054517 (2019).

[42] A. E. Böhmer, K. Kothapalli, W. T. Jayasekara, J. M. Wilde, B. Li, A. Sapkota, B. G. Ueland, P. Das, Y. Xiao, W. Bi, J. Zhao, E. E. Alp, S. L. Bud'ko, P. C. Canfield, A. I. Goldman, and A. Kreyssig, Distinct pressure evolution of coupled nematic and magnetic orders in FeSe, Phys. Rev. B **100**, 064515 (2019).

[43] P. S. Wang, S. S. Sun, Y. Cui, W. H. Song, T. R. Li, R. Yu, H. Lei, and W. Yu, Pressure induced stripe-order antiferromagnetism and first-order phase transition in FeSe, Phys. Rev. Lett. **117**, 237001 (2016).

[44] U. S. Kaluarachchi, V. Taufour, A. E. Böhmer, M. A. Tanatar, S. L. Bud'ko, V. G. Kogan, R. Prozorov, and P. C. Canfield, Nonmonotonic pressure evolution of the upper critical field in superconducting FeSe, Phys. Rev. B **93**, 064503 (2016).

[45] K. Rana, L. Xiang, P. Wiecki, R. A. Ribeiro, G. G. Lesseux, A. E. Böhmer, S. L. Bud'ko, P. C. Canfield, and Y. Furukawa, Impact of nematicity on the relationship between antiferromagnetic fluctuations and superconductivity in $FeSe_{0.91}S_{0.09}$ under pressure, Phys. Rev. B **101**, 180503 (2020).

[46] K. Rana, D. V. Ambika, S. L. Bud'ko, A. E. Böhmer, P. C. Canfield, and Y. Furukawa, Interrelationships between nematicity, antiferromagnetic spin fluctuations, and superconductivity: Role of hotspots in $FeSe_{1-x}S_x$ revealed by high pressure ^{77}Se NMR study, Phys. Rev. B **107**, 134507 (2023).

[47] T. Chen, Y. Chen, A. Kreisel, X. Lu, A. Schneidewind, Y. Qiu, J. T. Park, T. G. Perring, J. R. Stewart, H. Cao, R. Zhang, Y. Li, Y. Rong, Y. Wei, B. M. Andersen, P. J. Hirschfeld, C. Broholm, and P. Dai, Anisotropic spin fluctuations in detwinned FeSe, Nat. Mater. **18**, 709 (2019).

[48] Y. Yamakawa and H. Kontani, Nematicity, magnetism, and superconductivity in FeSe under pressure: Unified explanation based on the self-consistent vertex correction theory, Phys. Rev. B **96**, 144509 (2017).

[49] A. B. Morfoot, T. K. Kim, M. D. Watson, A. A. Haghighirad, S. J. Singh, N. Bultinck, and A. I. Coldea, Resurgence of superconductivity and the role of d_{xy} hole band in $FeSe_{1-x}Te_x$, Commun. Phys. **6**, 362 (2023).

[50] R. Khasanov, Z. Guguchia, A. Amato, E. Morenzoni, X. Dong, F. Zhou, and Z. Zhao, Pressure-induced magnetic order in FeSe: A muon spin rotation study, Phys. Rev. B **95**, 180504 (2017).

[51] M. Bendele, A. Amato, K. Conder, M. Elender, H. Keller, H.-H. Klauss, H. Luetkens, E. Pomjakushina, A. Raselli, and R. Khasanov, Pressure induced static magnetic order in superconducting $FeSe_{1-x}$, Phys. Rev. Lett. **104**, 087003 (2010).

[52] M. Bendele, A. Ichsanow, Y. Pashkevich, L. Keller, T. Strässle, A. Gusev, E. Pomjakushina, K. Conder, R. Khasanov, and H. Keller, Coexistence of superconductivity and magnetism in $FeSe_{1-x}$ under pressure, Phys. Rev. B **85**, 064517 (2012).

[53] F. Rullier-Albenque, D. Colson, A. Forget, and H. Alloul, Hall effect and resistivity study of the magnetic transition, carrier content, and Fermi-liquid behavior in $Ba(Fe_{1-x}Co_x)_2As_2$, Phys. Rev. Lett. **103**, 057001 (2009).

[54] M. Nakajima, S. Ishida, T. Tanaka, K. Kihou, Y. Tomioka, T. Saito, C. H. Lee, H. Fukazawa, Y. Kohori, T. Kakeshita, A. Iyo, T. Ito, H. Eisaki, and S. Uchida, Normal-state charge dynamics in doped $BaFe_2As_2$: Roles of doping and necessary ingredients for superconductivity, Sci. Rep. **4**, 5873 (2014).

[55] M. Rotter, M. Tegel, and D. Johrendt, Spin-density-wave anomaly at 140 K in the ternary iron arsenide $BaFe_2As_2$, Phys. Rev. B **78**, 020503 (2008).

[56] Z. Zajicek, I. Paulescu, and A. I. Coldea, Dataset - Drastic field-induced resistivity upturns as signatures of unconventional magnetism in superconducting iron chalcogenides, University of Oxford (ORA) (2026), https://dx.doi.org/10.5287/ora-dxkyaxjzy.